Optics Letters

High-finesse sub-GHz-resolution spectrometer employing VIPA etalons of different dispersion

Kim Berghaus,[1,2] Jitao Zhang,[2] Seok H. Yun,[1] and Giuliano Scarcelli[1,2,*]

[1]Harvard Medical School and Wellman Center for Photomedicine, Massachusetts General Hospital, 65 Landsdowne Street, Cambridge, Massachusetts 02139, USA
[2]Fischell Department of Bioengineering, University of Maryland, College Park, Maryland 20742, USA
*Corresponding author: scarc@umd.edu

Received 20 July 2015; revised 28 August 2015; accepted 31 August 2015; posted 1 September 2015 (Doc. ID 246287); published 23 September 2015

We report a novel configuration of a two-stage virtually imaged phased array spectrometer that enables high-throughput sub-GHz spectroscopy at a high finesse (>750). Two etalons with different free spectral range and different dispersion are arranged in an orthogonal direction and spread the spectrum across two dimensions, with a greatly improved rejection ratio of white-light background noise. A proof-of-concept application for Brillouin spectroscopy is demonstrated.

OCIS codes: (300.6190) Spectrometers; (290.5830) Scattering, Brillouin.

http://dx.doi.org/10.1364/OL.40.004436

Ultrahigh-resolution spectrometers with a resolving power better than 1 GHz ($0.03 \times \mathrm{cm}^{-1}$) [1] are essential for many applications, including Brillouin spectroscopy, low-frequency Raman spectroscopy, and comb-resolved analysis [1,2]. Fabry–Perot (FP) interferometers have been widely used to achieve sub-GHz spectral resolutions [3]. More recently, angle-dispersed virtually imaged phased array (VIPA) [4] has been introduced to attain similar resolutions with much higher throughput efficiencies [5]. Both FP and VIPA spectrometers achieve high spectral dispersion through the interference of multiple reflections between either two parallel mirrors or two interfaces of a solid etalon. An important figure of merit of a spectrometer is the *finesse*—the ratio of the adjacent fringes and the linewidth—which expresses the number of resolvable frequency components in a spectrometer. Finesse can be computed by the ratio of the frequency range that can be analyzed without ambiguity, termed free spectral range (FSR), and the spectral resolution of the spectrometer. The finesse of a spectrometer using free-space etalons is limited by the reflectivity and flatness of the reflecting surfaces. Practically, it is very difficult to surpass a finesse of 50.

Here, we present a sub-GHz spectrometer based on the principle of cross-axis spectrometry [6] but employing etalons of different spectral dispersion. Due to the different FSRs of the two orthogonal etalons, the spectral signatures are spread across two dimensions rather than on the conventional single axis. As a result, sub-GHz resolution is achieved together with a finesse greater than 750, an order of magnitude improvement over previously attainable values, and a more than tenfold improved rejection of white-light background noise. We demonstrated the advantageous features of such a spectrometer in the context of Brillouin spectroscopy [7–11].

A solid VIPA etalon has three different coating areas. The front surface has a highly reflective coating (R1) with a narrow anti-reflection coating strip (R3). The back surface has a partially reflective coating (R2). In order to use the VIPA as a spectrometer, a cylindrical lens is used to focus a light beam onto a tilted VIPA etalon through the narrow anti-reflection coating strip. Within the etalon, the beam is reflected and split into several subcomponents with fixed phase differences. The interference among these components introduces high spectral dispersion, and different frequency components are emitted at different angles. Passing the dispersed beam through another lens spatially separates the different frequency components of the beam in the focal plane of the lens. For higher spectral extinction, a two-stage VIPA spectrometer, where two VIPAs are aligned in an orthogonal direction, has been developed (Fig. 1) [5].

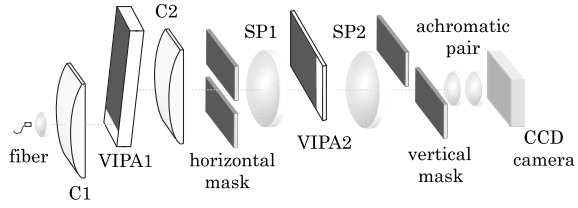

Fig. 1. Schematic of the two-stage VIPA spectrometer setup. In the first stage, the cylindrical lens C1 ($f = 200$ mm) inputs light into the VIPA (FSR = 20 GHz, $R1 = 100\%$, $R2 = 95\%$). The beam is focused by C2 ($f = 200$ mm), and a spatial mask blocks the undesired frequencies. In the second stage, a spherical lens ($f = 200$ mm) inputs light into VIPA2 (FSR = 13 GHz, $R1 = 100\%$, $R2 = 95\%$), aligned in an orthogonal direction; another spherical lens ($f = 200$ mm) focuses light onto a spatial mask. Finally, an achromatic pair ($f = 30$ mm) images the spectral pattern onto the CCD camera.

Figure 2 illustrates cartoons of typical spectral patterns of a two-stage VIPA spectrometer. In these cartoons, the point o represents the position of the laser beam or the unshifted elastic scattering; all other signals are dispersed in the two-dimensional plane due to their frequency shift with respect to the laser. The length of the square represents the value of the FSR in the corresponding direction. The two VIPAs disperse incoming light along their spectral axes in sequence; since their spectral axes are orthogonal, the overall spectral axis lies along a diagonal direction. Employing two VIPAs of the same FSR yields a single spectral dispersion axis oo', and the effective FSR is the same as that of a single VIPA [Fig. 2(a)]. However, the situation is different if two VIPAs have different FSRs, as shown in Fig. 2(b), where we have taken $\mathrm{FSR}_x/\mathrm{FSR}_y = 2/3$. If f_{CGD} is the greatest common divider (GCD) frequency of the two FSRs, we can write $\mathrm{FSR}_x = 2f_{\mathrm{CGD}}$ and $\mathrm{FSR}_y = 3f_{\mathrm{CGD}}$ (in units of GHz). In this case, the dispersed signal will lie along the spectral axis oa (blue diagonal line). When the frequency shift equals FSR_x, the signal will be at point a. For frequency shifts higher then FSR_x but smaller than FSR_y, the dispersed signal will move along spectral axis ab: in fact, the signal falls into the next diffraction order of the horizontal VIPA (and is thus "folded" onto the previous order) but in the same order of the vertical VIPA. For higher-frequency shifts, the signal will go through multiple spectral axes until it arrives at point o', where the frequency shift will be a multiple of both FSR_x and FSR_y. Thus, the effective FSR [Fig. 2(c)] can be understood graphically by unfolding the multiple spectral axes. In the previous example, the effective FSRs will be $\mathrm{FSR}_{\mathrm{eff}} = 3\mathrm{FSR}_x = 2\mathrm{FSR}_y = 6f_{\mathrm{CGD}}$ (in units of GHz). In general, the effective FSR of this configuration is given by the lowest common multiple of the single VIPA's FSR,

$$\mathrm{FSR}_{\mathrm{eff}} = \frac{\mathrm{FSR}_x \cdot \mathrm{FSR}_y}{f_{GCD}}, \tag{1}$$

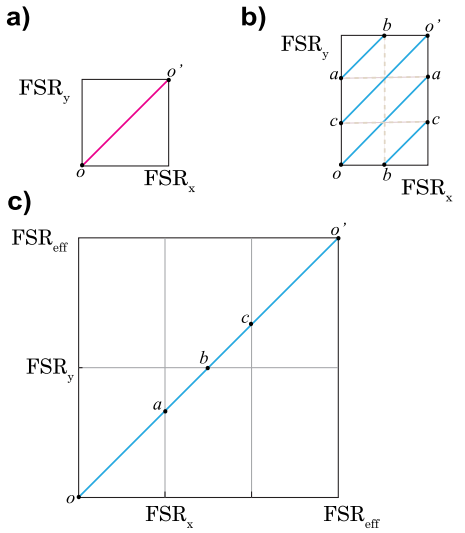

Fig. 2. (a) The dispersion pattern of a conventional two-stage VIPA spectrometer ($\mathrm{FSR}_x/\mathrm{FSR}_y = 1$); the spectrum is spread along one axis on the diagonal (pink line). (b) If the FSRs are different (e.g., $\mathrm{FSR}_x/\mathrm{FSR}_y = 2/3$), several spectral axes (blue lines) are observed. (c) The effective FSR after unfolding the spectral axes is $\mathrm{FSR}_{\mathrm{eff}} = 3\mathrm{FSR}_x = 2\mathrm{FSR}_y$.

where f_{CGD} has a value of the GCD of FSR_x and FSR, and all the parameters in Eq. (1) are in units of GHz.

Reading the spectrum in the new configuration requires a straightforward calculation: the spatial location (x, y) of a spectral signal within the pattern is determined by Eqs. (2a) and (2b),

$$x = (\nu - n_x \cdot \mathrm{FSR}_x)/\eta, \tag{2a}$$

$$y = (\nu - n_y \cdot \mathrm{FSR}_y)/\eta, \tag{2b}$$

where ν is the frequency shift, n_x and n_y are even integers, FSR_x and FSR_y are the values of the FSR of respective direction, and η is the spatial dispersion factor in units of GHz/pixels. Equations (2a) and (2b) can be graphically solved to find the frequency shift ν.

In practice, a much larger range of frequencies can be differentiated because the spectral signatures are located on separate dispersion axes. Without changing the spectral resolution of the spectrometer, the effective FSR is increased significantly. This leads to an effective increase of the overall number of resolvable frequency components without affecting the throughput of the spectrometer.

To illustrate the principle and features of the spectrometer, experimental measurements of Brillouin scattering of several materials were performed using a standard epi-detection Brillouin microscope [5]. Briefly, a 532 nm single-frequency laser light passed through a neutral density filter and a beam splitter. It was then focused onto the sample via an aspheric lens (focal length 11 mm), which also collected the backward scattered light. An objective lens ($f = 6$ mm) coupled the light into a single mode fiber, which served as confocal pinhole and delivered the light into the VIPA spectrometer. The illumination power at the sample was around 3 mW, and typical acquisition times were less than a second. The traditional spectrometer had an FSR_x and FSR_y of 20 GHz, which resulted in an effective FSR of 20 GHz. The new spectrometer had an FSR_x of 13 GHz and an FSR_y of 20 GHz, which resulted in an effective FSR of 260 GHz. This dramatic increase in the effective FSR of the spectrometer was particularly advantageous for Brillouin scattering analysis, where the frequency shift of the Stokes peak is the negative of the anti-Stokes peak, as shown in Fig. 3.

The Brillouin spectra of methanol (~5.6 GHz) and water (~7.5 GHz) are shown in Figs. 3(a) and 3(b). As their Brillouin shift is less than half the etalon FSR, a standard two-stage spectrometer had no issue in the analysis of their spectra. The situation was different in Fig. 3(c), where the Brillouin shift of mineral oil (~9.7 GHz) is shown. In the traditional setup, the Stokes and anti-Stokes peaks overlapped, which made it impossible to determine the Brillouin shift of mineral oil with accuracy. Instead, in the new setup, the two peaks were spatially separated within the two-dimensional plane and could be easily resolved.

Figure 3(d) shows the Brillouin spectrum of polystyrene (~14.2 GHz). In the traditional setup, the reading of the polystyrene shift along the single spectral axis was ambiguous, as the Brillouin shift is bigger than half the FSR; in the new setup, the shift was easily identifiable, as the location of the spectral signature within the two-dimensional plane was unique. Due to the expanded effective spectral range of

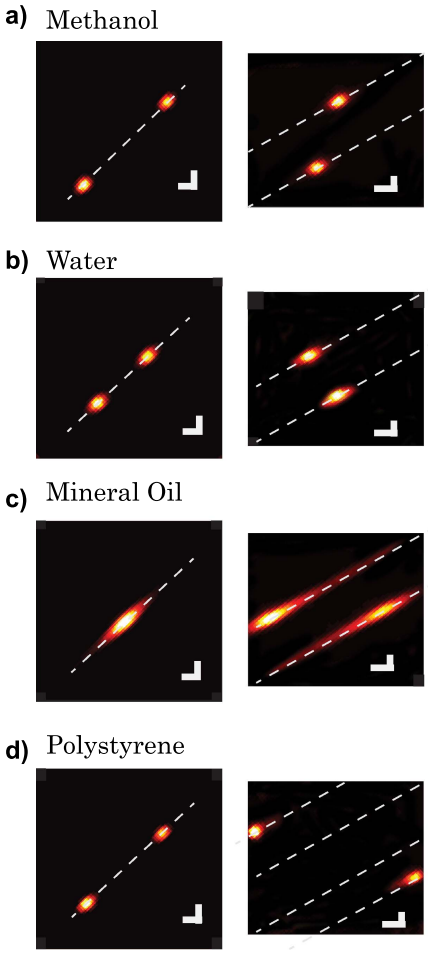

Fig. 3. Comparisons of the conventional (left panels) versus the new spectrometer configuration (right panels) Brillouin spectral patterns are shown for several materials: (a) methanol, (b) water, (c) mineral oil, and (d) polystyrene. For illustration purposes we drew a white, dashed line to indicate the spectral dispersion axis, and enhanced the spectral coloring with a Gaussian low-pass filter. Scale bars, 2 GHz.

FSR_{eff}, a unique position for Brillouin frequency shifts upward to $FSR_{eff}/2$ (the factor of 2 comes from the existence of Stokes and Anti-stokes peaks); in other words, 130 GHz became possible.

To estimate finesse, we divided the spacing between the laser signatures of adjacent diffraction orders by their linewidth. The traditional spectrometer featured a finesse of 30. The new spectrometer featured a finesse of 780, made up of single-stage finesses of 26 and 30. An important consequence of great practical value of the high spectrometer finesse is the superior rejection of noise coming from spectrally broad sources, such as white light or fluorescence. This is important because while traditional double-VIPA spectrometers provide sufficient (~60 dB) rejection of laser-related noise sources, they cannot deal with noise sources featuring a broad spectrum. To quantify this improvement, white light was applied from a microscope lamp directly onto the sample. Figure 4(a) shows two representative images of a Brillouin signal from methanol in the presence of white-light noise. By spreading the broad noise source across two dimensions, the background noise was clearly reduced. The drop in background noise level was measured to be 11 dB in the new spectrometer [Fig. 4(b)]. To characterize this feature in terms of signal-to background ratio (SBR), the intensity of the white light was quantified using a separate camera while blocking the laser. Figure 4(c) displays the inverse of the SBR versus the intensity of the illumination. The *x*-axis was normalized to the maximum illumination used, which corresponds to about 75% of the full power of a standard lamp on a bright-field microscope. The SBR was determined by dividing the half-width integral of the actual signal by its background, where the actual signal is the measured signal minus background. The error bar was estimated by the standard deviation of repeated measurements. The background below the signal was estimated by curve fitting. Since the Brillouin signal remained constant, as expected, we observed a linear behavior of 1/SBR, as shown in Fig. 4(c).

In addition, the increased rejection ratio corresponds with our expectations. If we look at the upper limit of the background illumination that the spectrometer can handle

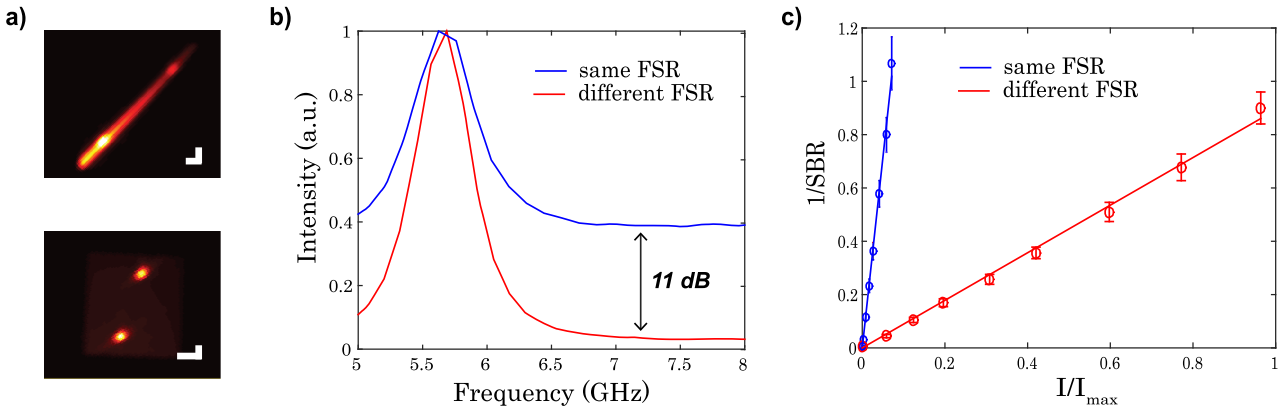

Fig. 4. (a) CCD images of Brillouin spectral patterns of methanol in the presence of white-light background in a traditional two-stage VIPA spectrometer (i.e., with the same FSR) (top) versus our novel configuration featuring etalons of different FSRs (bottom). Scale bars, 2 GHz. (b) Comparison of the Brillouin spectrum of methanol in same-FSR (blue) versus different-FSR (red) configurations. (c) The inverse of the signal-to-background ratio versus illumination shows an improvement in background suppression by a factor of 16. The *x*-axis is normalized to the maximum illumination used.

(SBR = 1), it is evident that the new configuration rejects background much more effectively than the conventional spectrometer. Experimentally, a factor of 16 was obtained from the ratio of the slopes from the two curves displayed in Fig. 4(c), which is about half the value of the single-stage finesse. The finesse of the second stages determines the signal spread in the opposite directions; the factor of 2 is due to folding of negative and positive frequency shifts of white light around the Brillouin signal. Following similar principles of combining spectral elements of different dispersions, VIPA etalons have been used together with gratings and obtained impressive results for two dimensional spectral and spatial mapping [1,12–14]; however, these spectrometers are not suitable for Brillouin and/or low-frequency Raman applications as their spectral extinction is equivalent to a single-etalon VIPA spectrometer (~30 dB).

In conclusion, we have developed a novel two-stage VIPA spectrometer with etalons of different FSRs that yield a high finesse, greater than 750, and more than tenfold improved background extinction compared to two-stage VIPA spectrometers with etalons of equal FSR. For Brillouin spectroscopy applications, this novel configuration greatly improves the number of unambiguously resolvable frequency components, allows us to perform Brillouin spectral measurements of fluorescent samples, and enables combinations with other imaging modalities, such as bright-field or fluorescence microscopy.

Funding. Human Frontier Science Program (HFSP) (Young Investigator Grant); MSIP (Ministry of Science, ICT and Future Planning), Korea, "ICT Consilience Creative Program" (IITP-2015-R0346-15-1007); National Eye Institute (NEI) (R21 EY023043); National Institute of Biomedical Imaging and Bioengineering (NIBIB) (K25 EB015885, P41 EB015903).

REFERENCES

1. S. A. Diddams, L. Hollberg, and V. Mbele, Nature **445**, 627 (2007).
2. G. Scarcelli and S. Yun, Nat. Photonics **2**, 39 (2007).
3. J. R. Sandercock, RCA Review **36**, 89 (1975).
4. M. Shirasaki, Opt. Lett. **21**, 366 (1996).
5. G. Scarcelli and S. Yun, Opt. Express **19**, 10913 (2011).
6. G. Scarcelli, P. Kim, and S. Yun, Opt. Lett. **33**, 2979 (2008).
7. G. Scarcelli, P. Kim, and S. Yun, Biophys. J. **101**, 1539 (2011).
8. G. Scarcelli, S. Besner, R. Pineda, P. Kalout, and S. Yun, JAMA Ophthalmol. **133**, 480 (2015).
9. S. Reiss, G. Burau, O. Stachs, R. Guthoff, and H. Stolz, Biomed. Opt. Express **2**, 2144 (2011).
10. Z. Meng, A. Traverso, and V. Yakovlev, Opt. Express **22**, 5410 (2014).
11. G. Antonacci, M. Foreman, C. Paterson, and P. Torok, Appl. Phys. Lett. **103**, 221105 (2013).
12. V. Supradeepa, C. Huang, D. Leaird, and A. Weiner, Opt. Express **16**, 11878 (2008).
13. K. Goda, K. K. Tsia, and B. Jalali, Nature **458**, 1145 (2009).
14. C. Wang, Z. Ding, S. Mei, H. Yu, W. Hong, Y. Yan, and W. Shen, Opt. Lett. **37**, 4555 (2012).